Supporting Information: Materials and Methods, and Figures

In this appendix we describe the experimental and theoretical methods used to understand the dispersion of particles sprinkled onto the surface of a liquid. In our experiments, particles were sprinkled onto a liquid surface using a forceps or spatula. The subsequent motion of trapped particles was recorded using a digital video camera mounted above the surface. In our theoretical studies, the direct numerical simulation (DNS) approach and the force balance equation for a particle trapped at the interface were used to understand the underlying physics.

A.1. Experimental method and results

There are several factors that determine whether a particle dropped onto the surface of a liquid will sink or float. First, the vertical capillary force must be large enough to balance the particle's buoyant weight. The vertical capillary and pressure forces must also overcome the momentum of the particle, which it possesses before coming in contact with the liquid surface. Since the capillary force acting on a particle varies linearly with the particle size and the buoyant weight and the momentum vary as the third power of the particle radius [4,7], small particles are more easily captured at the interface. Furthermore, to reduce the momentum at impact, particles were dropped from a distance of a few millimeters above the interface.

The liquids used in this study were water, corn oil and glycerin. The presence of contaminants on the air-water interface, even when their concentration is very small, can alter the interfacial tension and the contact angle of the water. To address this problem, we used Millipore water. The size of particles was selected so that they would float. In most of the experiments, particles were spherical; they were dried for several hours at the temperature of 70º C in an oven to eliminate the influence of any residual moisture. Moisture is important because it can influence the contact angle and thus the position of the three phase contact line on the particle's surface. In Figure S1, we have shown the top views of two floating glass particles of nearly the same size shortly after they were trapped at the air-water interface. The particle which was dried for several hours was more hydrophobic, so that it floated with more of its surface in the air; even a slight amount of moisture on the surface of a particle can influence the contact angle. After a few minutes the exposed areas for both particles in Figure S1 became similar. Since the dispersion phase of the motion of particles sprinkled onto a liquid surface is very short, the surface moisture influences the velocity with which particles disperse. Therefore, for all of the cases for which

quantitative data are reported in this paper, particles and powders were dried in an oven to eliminate the influence of the day-to-day variation of the humidity on the dispersion of particles.

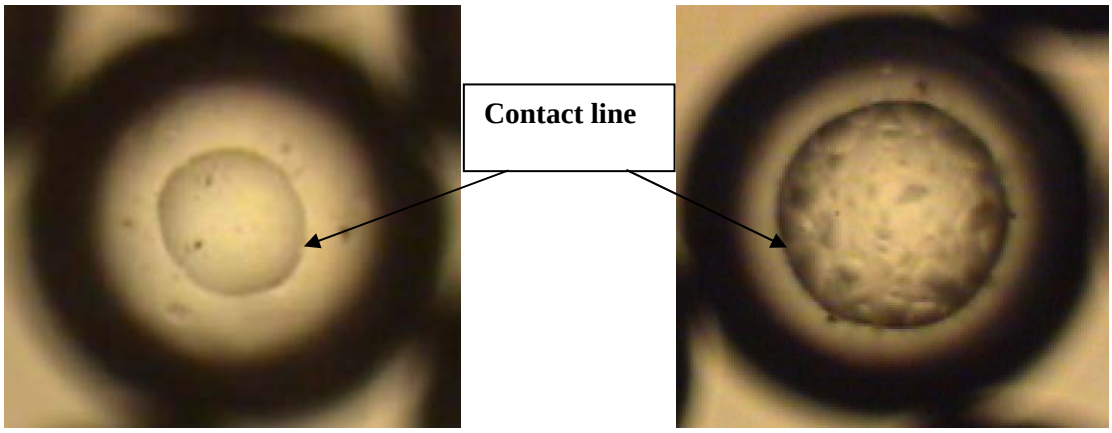

(a) (b)

Figure S1. Photographs of glass particles floating on the air-water interface (taken from above the surface) showing the influence of humidity on the contact line. The diameter of particles was 550 μm. (a) A particle that was kept under normal room conditions, (b) A particle that was kept in an oven at 70º C for 24 hours. The area exposed to air is larger in (b) and so the dried particle is more hydrophobic.

In our experiments one, two or more particles were dropped onto a liquid surface simultaneously. The lateral velocity of particles after they were trapped at the interface was calculated by analyzing the video recordings. We used glass particles with diameter between 450 μm and 1.1 mm, and mustard seeds of ~1.1 mm diameter. All of these particles were captured within the interface.

When a particle comes in contact with a liquid surface it experiences a strong vertical force due to capillarity which acts to bring the particle to its equilibrium height within the interface. The equilibrium height can be defined as the distance between the center of mass of the particle and the undisturbed liquid surface (before the particle was sprinkled). The equilibrium height is determined by a balance of the buoyant weight and the vertical interfacial force, and the contact angle which determines the latter force.

Our experiments show that when a single spherical particle is dropped onto a liquid surface it causes the fluid around it to move away. We call the dropped particle a test particle. The particle itself, of course, does not move laterally on the interface. To investigate the fluid motion caused by a test particle, the interface was seeded with 100 μm sized glass particles. Since the size of these seeded particles was several times smaller than that of the test particle, we may assume that

they acted approximately as tracer particles and their motion can be used to deduce the local fluid velocity caused by dropping a larger particle. The size of tracer particles compared to that of a test particle, and the field of view/magnification for the camera, were selected so that the motion of tracer particles within several diameters of the test particle could be monitored. Also, although the number density of tracer particles at the interface was kept small to ensure that they did not influence the fluid motion caused by the test particle, it was large enough to measure the fluid velocity at a sufficient number of points at various distances from the test particles.

A.1.1 One particle

Figure S2 shows the velocity of tracer particles, as a function of the distance from the center of a test glass particle of 850 μm diameter, 0.033 s after contact with the air-water interface. The experiment was repeated for several different spherical particles of the same approximate diameter. After a test particle was trapped at the interface, all of the nearby tracer particles on the air-water interface moved outward from the center of the test particle. The figure shows that the velocity of tracer particles decreased with increasing distance from the test particle. The velocity data points do not fall on a single curve, but are spread about a mean curve. There can be several reasons for this spreading. The surface properties and the smoothness of particles used may be different. The contact line, soon after it was trapped at the interface, was not smooth (see Figure S1). There can also be a variation in the particle's rotational velocity, acquired when it was dropped onto the interface.

The velocity of tracer particles decreased with increasing time. For a tracer, initially at a distance of 2.05 mm from the center of the test particle, the velocity at t=0.8 s decayed to approximately zero (see Figure S3). As discussed below in section A.3, a particle of radius 1.0 mm attains a velocity of O(10) cm/s normal to the interface under the action of the vertical capillary force. Therefore, the time taken by it to travel a distance equal to its radius downwards is $O(10^{-2})$ s. The test particle, however, oscillates about its equilibrium height for a longer period before coming to a state of rest. The frequency of oscillation in our experiments for an 850 μm particle was around 55 Hz. An accurate measurement of the frequency for particles smaller than 850 μm was not possible using our present setup. Furthermore, the velocity of tracer particles near the dropped particle (~10 mm/s) was an order of magnitude smaller than the estimated value of the velocity of the test particle normal to the interface. A direct measurement of the latter velocity was not possible using our present experimental setup.

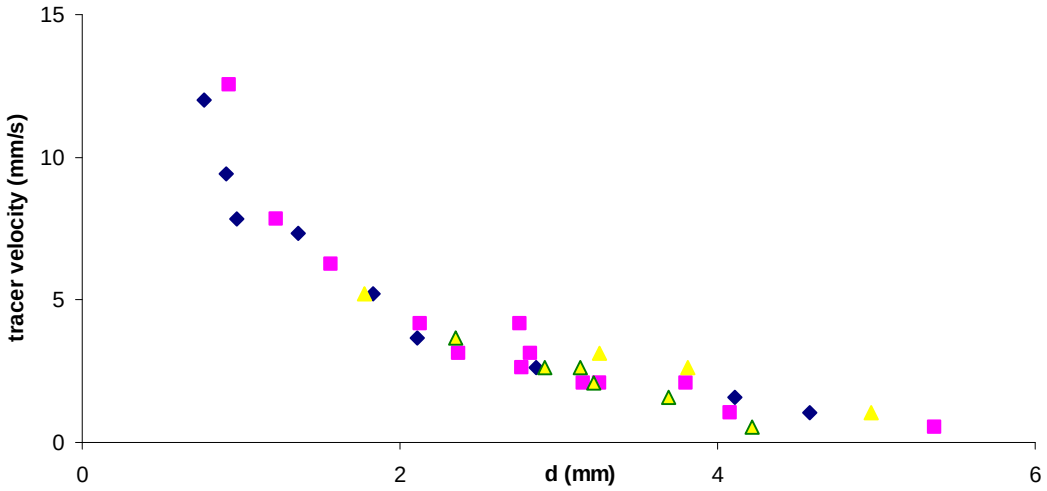

Figure S2. The velocity of tracer particles on the air-water interface is plotted as a function of the distance (d) from the center of a test glass particle. The velocity distribution plotted here is at a time 0.033 s after the particle was trapped at the interface. The data were taken for 7 different particles of the same approximate diameter of 850 μm.

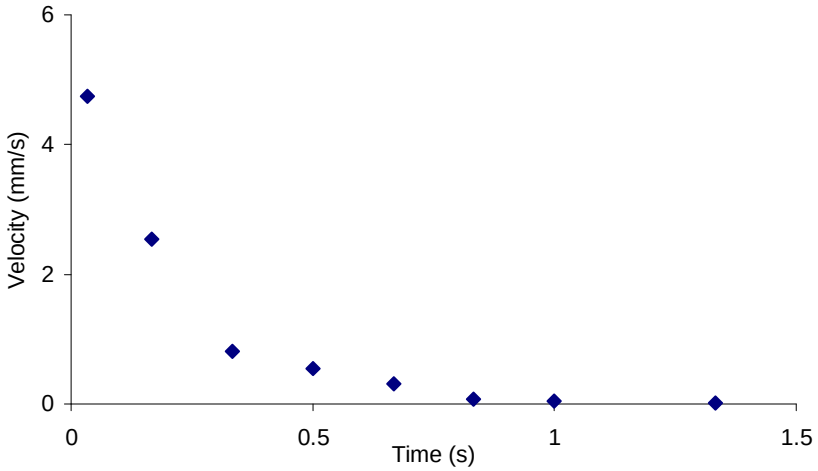

Figure S3. The velocity of a tracer particle on the air-water interface initially at a distance of 2.05 mm from a glass test particle of diameter 850 μm is shown as a function of time. The velocity became negligibly small at t = ~0.8 s.

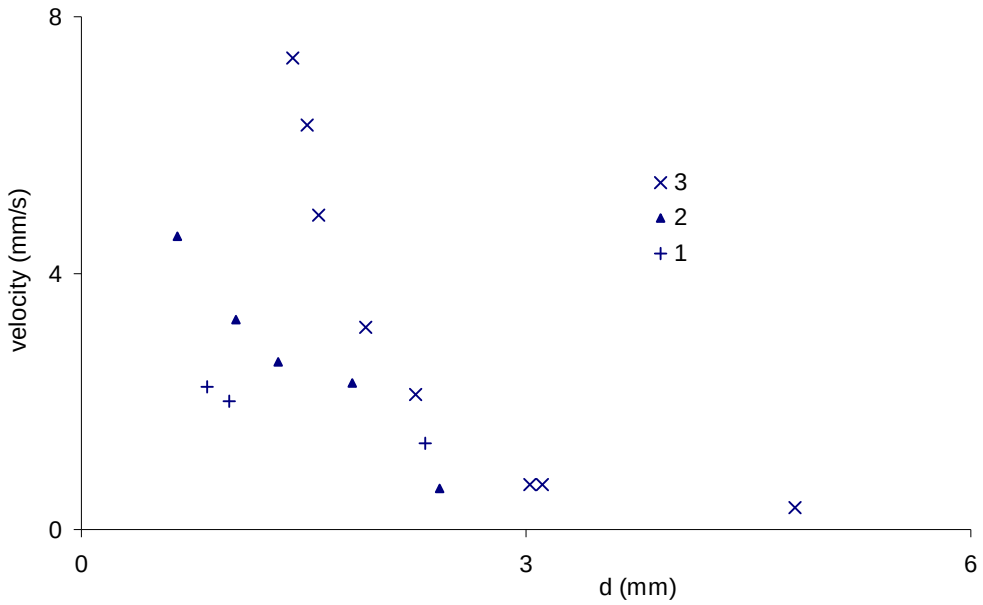

Figure S4. (a) The velocity of tracer particles on the surface of a mixture of 60% glycerin in water is shown as a function of the distance (*d*) from the center of a test particle. The velocity distribution here is at a time 0.033 s after the particle was trapped at the interface. The case marked "1" is for a glass sphere of diameter 850 μm, "2" is for a glass sphere of diameter 550 μm, and "3" is for a mustard seed of diameter 1.1 mm.

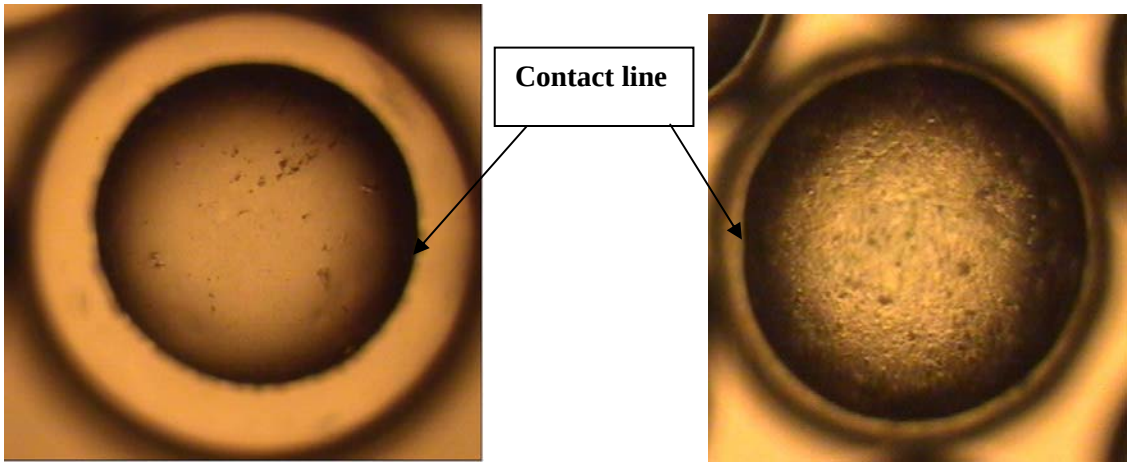

(i) diameter 850 μm (i) diameter 550 μm

Figure S4. (b) The contact line positions for glass particles floating on the surface of 60% glycerin in water are shown. Both particles were dried in an oven for one day. The fraction of the surface of an 850 μm particle exposed to air is smaller than that of 550 μm particle. The dispersion velocity is larger for the latter particles.

The above experiment was repeated for a mixture of 60% glycerin in water. The results obtained were qualitatively similar except for that the velocity of tracer particles was smaller. For example, Figure S4a shows that the velocity of tracer particles at a distance of 1 mm from the surface of a glass (test) particle of diameter 850 μm for glycerin was ~2 mm/s which is approximately 3 times smaller than on the air-water interface (see Figure S2). This is expected since the viscosity of 60% aqueous glycerin is about 6 times larger than that of water. The interfacial tension and the density of glycerin are also smaller. The velocity decayed to zero, 0.5 s after the particle was trapped at the interface. This time interval for 60% aqueous glycerin, as expected, is also shorter than for the air-water interface.

The velocity of tracer particles at a distance of 1 mm from the surface of a 550 μm glass test particle was ~3.5 mm/s, as shown in Figure S4a. The velocity induced by a 550 μm particle, therefore, was larger than that by an 850 μm glass particle. This could be due to the fact that the fraction of the particle's surface exposed to air was significantly larger for the 550 μm sized particle (see Figure S4b). The velocity induced due to a mustard seed, at a distance of 1 mm from the particle, was ~4.9 mm/s. This relatively large surface velocity due to a mustard seed is consistent with the fact that it also floated with approximately one half of its surface exposed to air. These results imply that the surface flow induced by the dropping of a particle is greater when it floats so that one half of its surface remains exposed to air. This is also consistent with our numerical results and the analysis presented in sections A2 and A3.

We next present results which show that the velocity of tracer particles on the air-water interface due to dropping of a test particle was approximately independent of the height from which the particle was dropped when the dropping height was varied between 3 mm to 8 mm. Our setup did not allow us to drop the particle from a smaller height. In Figure S5, the velocity of tracer particles at the distances of approximately 2 and 3 mm from the test particle is shown. The figure shows that the height from which the particles were dropped did not noticeably influence the velocity with which tracer particles moved away from the test particle.

The total distance traveled by a tracer particle (away from the test particle) depended on the initial distance from the test particle. Figure S6 shows that a tracer particle initially at a distance of 1 mm from a test particle of diameter 850 μm moved a distance of 3.4 mm and that this value decreased as the distance from the test particle increased. The former implies that a test particle creates a circular space free of tracer particles the radius of which can be more than four times the

test diameter. The latter is consistent with the result that the velocity of tracer particles decreased with increasing distance from the test particle.

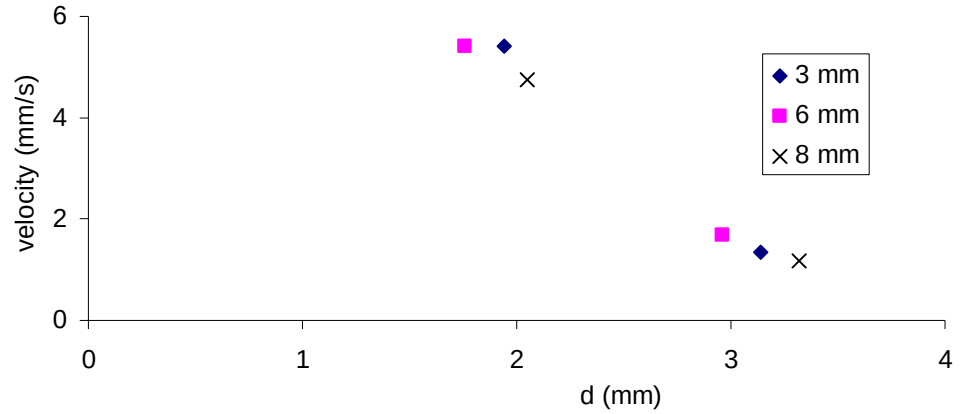

Figure S5. The velocity of tracer particles at the distances of ~2.0 and ~3.0 mm from the test particles on an air-water interface. The height from which the test particles were dropped was 3, 6 or 8 mm. The velocity values shown in this figure are at a time 0.033 s after the particle was trapped at the interface. The diameter of the test particles was 850 μm. Notice that the velocity of tracer particles was approximately independent of the height from which the particle was dropped.

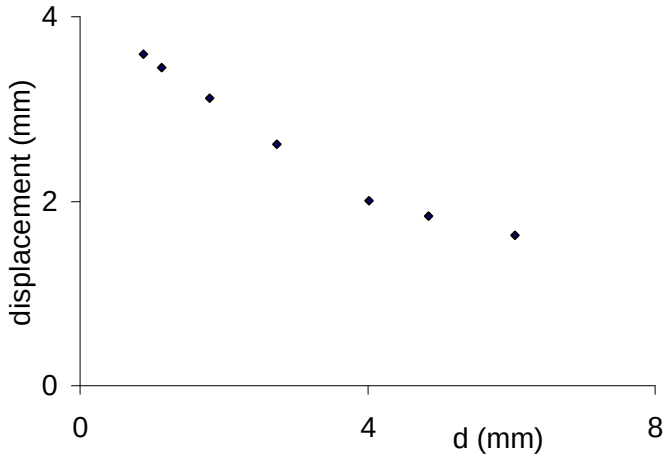

Figure S6. The distance traveled by tracer particles on the air-water interface is plotted as a function of their initial distance from the glass test particle. The diameter of the test particle was 850 μm and of a tracer particle was 100 μm.

A.1.2. Two particles

We next present results for the interfacial fluid velocity when two identical glass test particles were dropped simultaneously onto the air-water interface. The diameter of the test particles was 850 μm and the initial distance between them was about 910 μm. The motion of tracer particles in this case was radially outward from the middle of the line joining the centers of the test particles; the distance (d) of a tracer particle shown in Figure S7 was measured from this point. The velocity of tracer particles as a function of the distance (*d*) is shown along two mutually orthogonal directions. The inline direction is parallel to the line joining the centers of the test particles and the perpendicular direction is normal to this direction. For a given distance (*d*), the inline velocity was slightly larger.

Furthermore, the velocity of tracer particles in Figure S7 was larger than in Figure S2 where only one particle was dropped. This implies that the net flow induced at the interface (measured using tracer particles) is stronger when two particles were dropped. This is due to the fact that each particle creates its own radially outward flow, resulting in a net flow which can be approximated as the sum of the flows caused individually by the dropped particles. The other features of the induced flow were qualitatively similar to that for one particle.

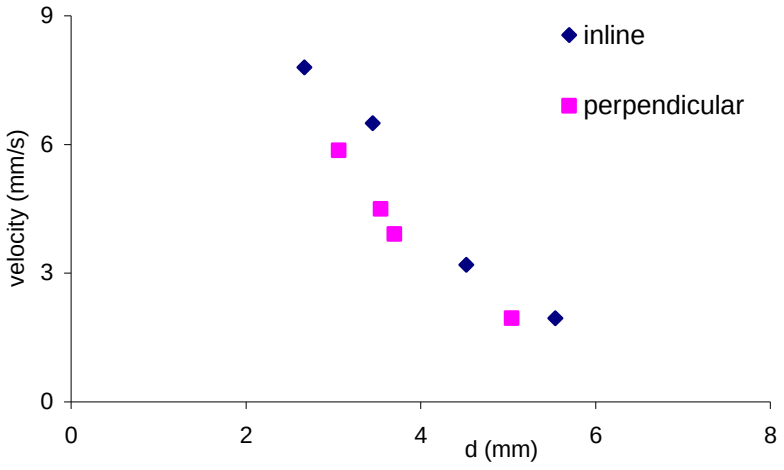

Figure S7. The velocity of tracer particles on the air-water interface is plotted as a function of the distance (d) from the mid-point of the line joining the centers of the two test particles. The diameter of the particles was 850 μm and the initial distance between them was 0.91 mm. The velocities shown here are at a time 0.033 s after the particles were trapped at the interface. The velocities of tracer particles are shown along the directions inline (parallel) and perpendicular to the line joining the particles centers.

After contact with the interface, the two test particles also moved away from each other along the line joining their centers. Figure S8 shows that the separation velocity decreased with increasing time, and decayed to approximately zero for t = 0.2 s; the velocities of the two particles were approximately equal in magnitude. The initial distance between the particles was varied to study its influence on the velocity of separation. Figure S9 shows that the relative velocity with which particles separated 0.033 s after contact, decreased with increasing initial distance between them. Furthermore, after some time particles reversed direction to came back to cluster under the action of attractive lateral capillary forces that arise because of the particles' buoyant weight. The velocity with which they came back however was significantly smaller than the velocity with which they dispersed.

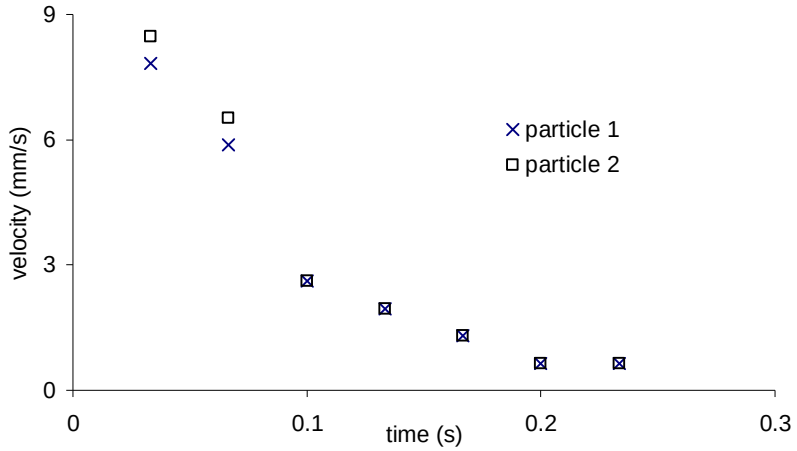

Figure S8. The velocity of two glass particles of diameter 850 μm dropped simultaneously onto the air-water interface is shown as a function of time. The initial distance between the particles was 1.21 mm. After becoming trapped in the interface, they moved apart other along the line joining their centers. The magnitudes of the velocities of the two particles were approximately equal.

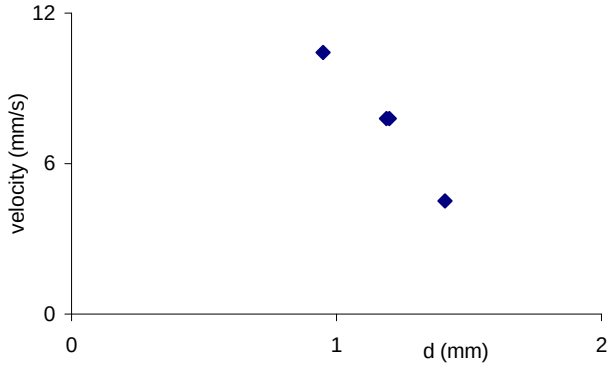

Figure S9. The average velocity with which two glass particles dropped together on the air-water interface moved apart along the line joining their centers is plotted against the initial distance between them. The velocities here are at a time 0.033 s after the particles came in contact with the interface. The diameter of particles was 850 μm.

The velocity with which two glass particles of the same size moved apart was larger than the velocity with which a tracer particle at the same separation moved away when a single glass particle was dropped. This is noteworthy because the larger glass particles have a larger mass, and so are expected to move slowly and not faster. However, they moved apart faster because of a repulsive hydrodynamic force that arises because of their motion in the direction normal to the interface (and so also perpendicular to the line joining their centers) (see Figure 2d). Specifically, when two particles are dropped onto the interface simultaneously, they are pulled downwards into the interface by the vertical components of the capillary forces. If the normal velocities are large, they overshoot equilibrium and oscillate about the equilibrium height before reaching a state of rest. This motion of particles in the direction perpendicular to the line joining their centers causes the fluid to squeeze through the gap in between them giving rise to the repulsive hydrodynamic force.

We also considered the case where a glass particle was dropped near an identical glass particle (which was already) trapped within the interface (see Figure S10). In this case, the trapped particle moved away along the line joining their centers, but the test particle did not move significantly. The particle that is dropped oscillates in the direction normal to the interface and thus creates a flow on the interface away from itself. The particle already at its equilibrium height moved away because of this flow. The velocity with which the trapped particle moved away decreased with increasing distance between the particles. Furthermore, the velocity of the glass particle was smaller than that of a tracer particle at a similar distance. This is not unexpected because the larger glass particles have a larger mass, and hence they move slowly.

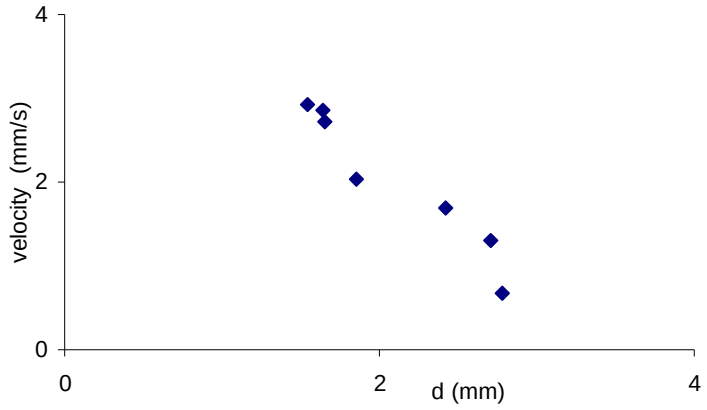

Figure S10. The velocity of a glass particle already on the air-water interface induced by dropping of an identical particle is shown as a function of the initial distance between the particles. The diameter of glass particles was 850 μm. The results are shown here are at a time 0.033 s after the particle was trapped on the interface.

A.1.3 Clusters of particles

We next describe the case when more than two particles were dropped onto a liquid surface. The goal is to determine the dependence of the dispersion velocity of particles on the number of particles. In Figure S11, we have plotted the velocities of four glass particles dropped together onto an air-water interface as a function of time. The diameter of these test particles was 650 μm. The particles moved apart along radial lines emanating from the center of the cluster. The velocities were different because the initial distances between the test particles were not the same and could not be controlled in our experiments. The average velocity with which the particles moved apart was larger for four than for two particles. This shows that the velocity with which particles dropped onto a liquid surface move apart depends on the number of particles dropped.

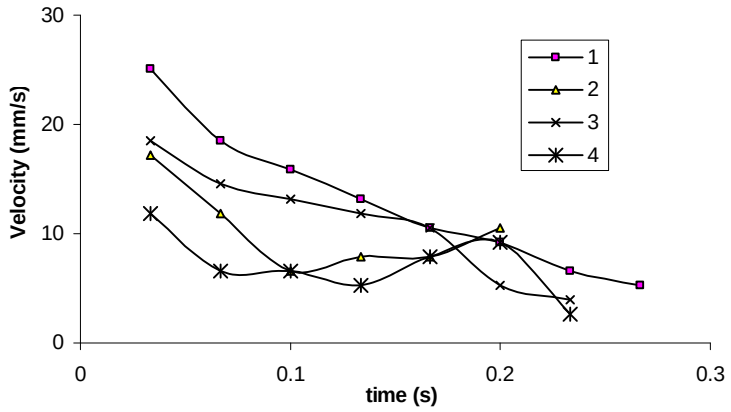

Figure S11. The velocities of four glass particles simultaneously dropped onto an air-water interface. The particles moved apart along radial lines emanating from the center of the four particles. The diameter of particles was 650 μm. The initial average distance between the four particles was around 1.0 mm.

To further investigate this increase in the average velocity of dispersion on the number of particles dropped, we considered the cases where a small number of particles, e.g., 2, 4, 8 or 16, were dropped simultaneously. In all of these cases, particles moved away from the center of the cluster after coming into contact with the interface. Video data were analyzed to obtain the

average dispersion velocity from their individual velocities. The experiment was repeated several times to obtain an average value of the dispersion velocity.

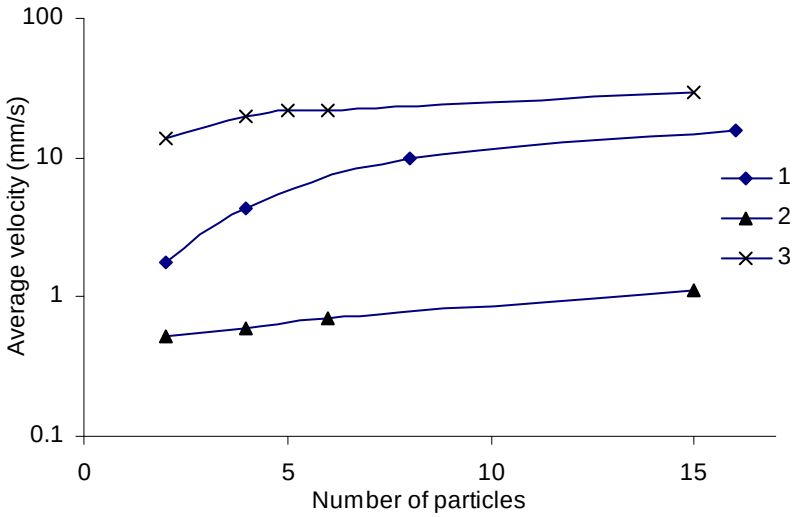

Figure S12. The average velocity with which glass particles on an interface moved apart 0.033 s after coming in contact as a function of the number of particles. The case marked "1" is for 850 μm glass particles sprinkled on water, "2" is for 650 μm glass particles sprinkled on 60% glycerin in water, and "3" is for 650 μm glass particles sprinkled on corn oil.

In Figure S12a, the average dispersion velocity on the air-water interface is shown as a function of the number of particles dropped. The figure shows that the average velocity increases with increasing number of particles. The same experiment was repeated to study the dispersion of test particles on air-corn oil and air-glycerin interfaces. The results for these latter studies also shown in Figure S12, are qualitatively similar.

We next describe the spreading behavior of glass powder sprinkled onto the air-water interface. The mean diameter of particles was 18 μm, and the density was 0.6 g/m^3. This powder was selected to ensure that a significant fraction of test particles would not sink. The number of particles dropped for this case was too large to count; hence the amount of powder sprinkled is described in terms of the weight.

The time taken by a given amount of powder to disperse into a disk shaped region of radius 1 cm is shown in Figure S13. For all of the cases considered, the initial area over which the powder was sprinkled was much smaller than of a circle with radius 1 cm. The time taken decreased when the amount of powder sprinkled increased which implies that the dispersion velocity increases with the amount of powder. For the cluster of the maximum weight considered in this figure, the dispersion velocity was ~ 3 cm/s. This velocity is several times larger than the velocity with

which the larger sized glass particles described in Figure S2 dispersed. Using our present setup it is not possible to simultaneously drop two particles onto the interface (near each other) if their diameter is smaller than ~400 μm, and so we were unable to study the spreading behavior of two 18 μm sized particles.

The radius of the region covered by the sprinkled powder continued to increase beyond 1 cm, but the rate of dispersion decreased with time before a steady maximum value was reached. In Figure S14, we have plotted the mean radius of the disk shaped region covered by the sprinkled powder against the amount of powder sprinkled. The radius increased with increasing amount of powder sprinkled until the expansion was inhibited by side walls of the dish.

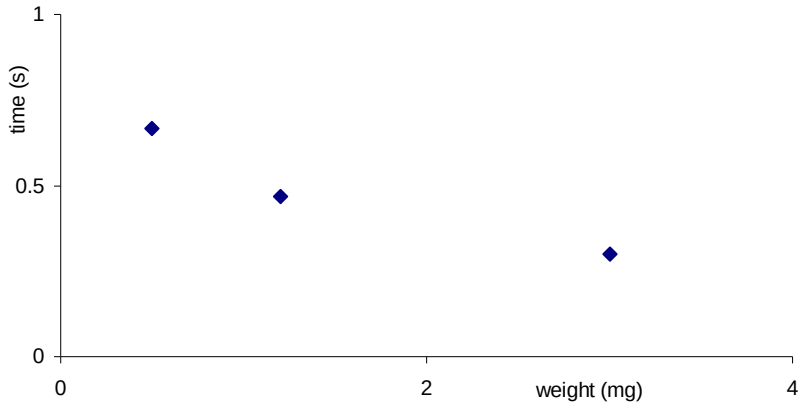

Figure S13. The time taken by the powder sprinkled onto the air-water interface to disperse to an approximately circular region of radius 1 cm is plotted against the amount of powder sprinkled. The area of the region over which the powder was sprinkled was relatively small. The average particle size was 18 μm and the density was 0.6 kg/m^3.

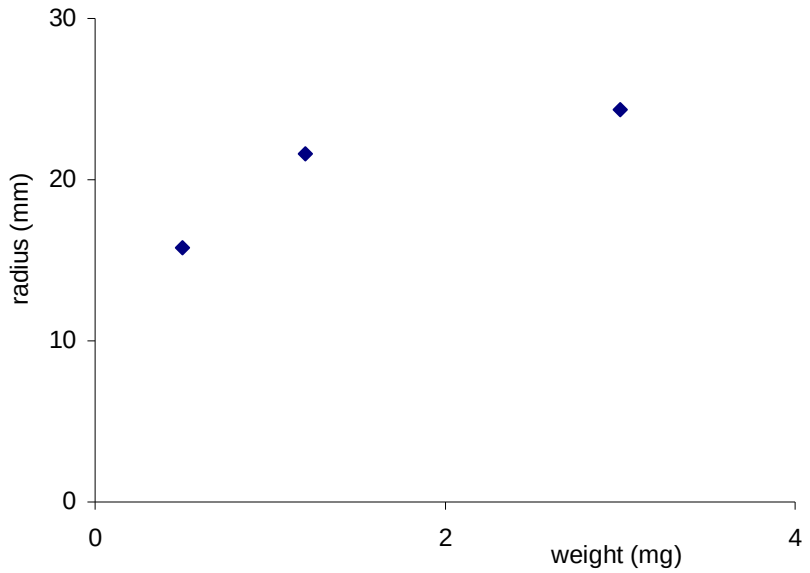

Figure S14. The final radius of the disk shaped region covered by the glass powder is plotted against the amount of powder sprinkled. The average particle size was 18 μm and the density was 0.6 kg/m^3.

We may therefore conclude that when more particles or a small amount of powder is sprinkled onto a liquid surface, each particle contributes to the outward dispersion of the cluster. The resulting flow on the interface can be approximated as the sum of the flows caused by them individually; therefore the dispersion velocity increases with increasing amount of powder sprinkled.

A.1.4 Velocity distribution within a cluster

To further understand the mechanism by which a group of particles sprinkled onto a liquid surface disperse, we created clusters of O(100) particles and measured their velocities as a function of the distance from the center of the cluster. We first describe the results for mustard seeds of diameter 1.1 mm sprinkled onto the air-water interface. In Figure S15, the average velocity of particles at various distances from the cluster center is plotted at three different times. At all three times the average velocity increased with increasing distance from the cluster center. In fact, the average velocity at a fixed time increased approximately linearly with increasing distance from the cluster center. Therefore, particles near the outer periphery of the cluster had the maximum velocity and those near the center had the minimum. This distribution of the velocity obviously implies that the cluster size increases with time. The average velocity decreased with increasing time as the rate of dispersion decreased. Similar results were obtained

when 26 mustard seeds were sprinkled (see Figure S15b), except that the data were much noisier and the maximum average velocity was smaller. The results for 80 glass beads of diameter 650 μm diameter on 99% glycerin in water are shown in Figure S15c. Again, the particle velocity increased with increasing distance from the cluster center, and decreased with increasing time. The average velocity for this case was smaller because the glycerin viscosity is larger.

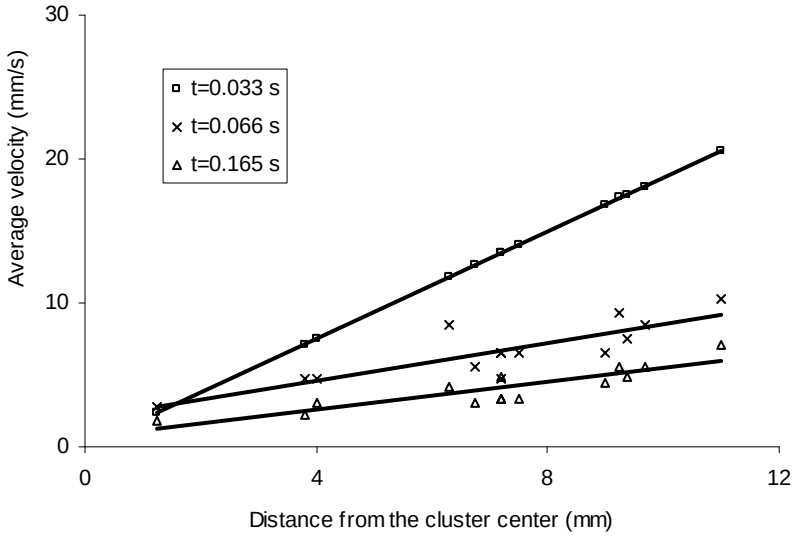

(a)

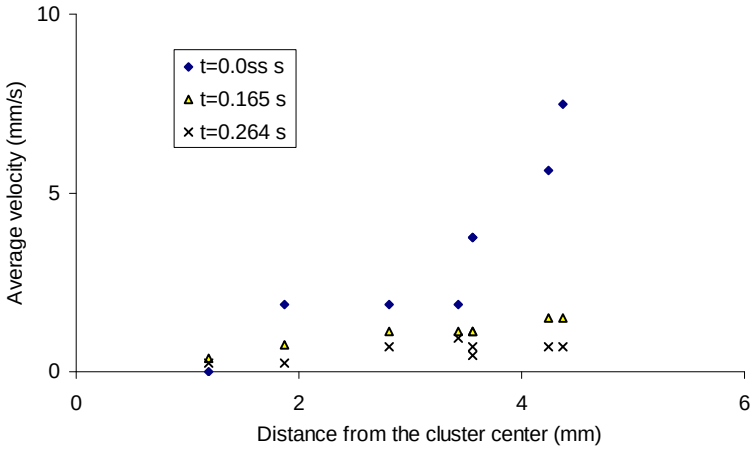

(b)

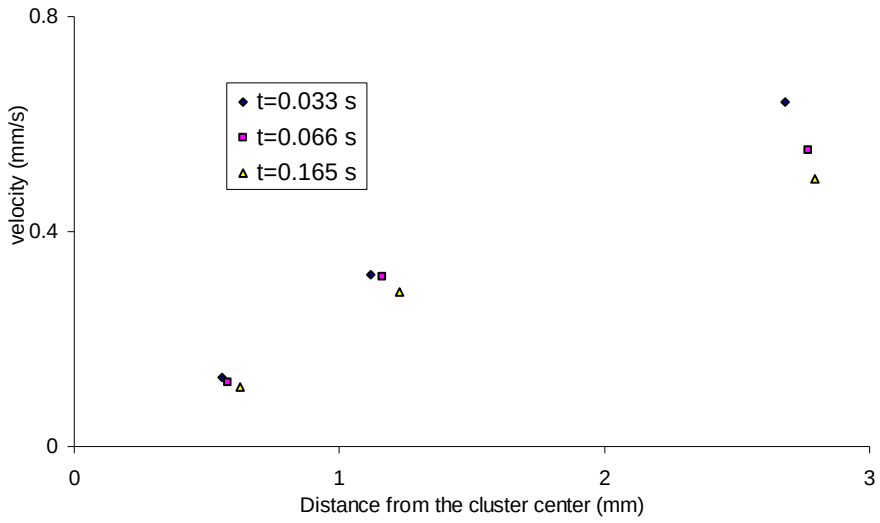

(c)

Figure S15. The radial particle velocity is shown as a function of the distance from the cluster center at three different times after they were sprinkled. (a) 76 mustard seeds were sprinkled onto the water surface. (b) 26 mustard seeds were sprinkled onto the water surface. (c) 80 glass spheres of 450 μm diameter were sprinkled onto the surface of 99% glycerin in water.

A.2. Direct Numerical Simulations (DNS)

We next present the results of our direct numerical simulations for the dispersion of particles trapped at a fluid-fluid interface. In our DNS approach, the details of which were described in [7], particles are moved according to the fundamental equations of motion of fluids and solid particles without the use of models. Specifically, the fluid-particle motion is resolved by the method of distributed Lagrange multipliers, the interface is moved by the method of level sets and the interface conditions are satisfied using the ghost fluid method [8-11]. The problem of the motion of a contact line on the surface of a particle is modeled using a phenomenological approach in which the contact angle given by the Young-Dupré law is prescribed. In this approach, the contact line on the surface of the particle is moved to maintain the prescribed value of the contact angle. This may not be the case for experiments, especially when the particle velocity is relatively large, if the contact angles for the advancing and receding contact lines are different form the value given by the Young-Dupré law. The initial positions of the particles in our simulations were such that the interface intersected the particles' surface.

We first present the case of two particles simultaneously released in a fluid-fluid interface. The particles centers were at a height of 0.95*R* above the undeformed interface. The initial shape of the interface was assumed to be flat and the contact line was assumed to be the intersection of the sphere with the flat interface. The latter was then evolved to satisfy the contact angle condition of 120º. As shown in Figure S16, the particles moved downwards under the action of the capillary and gravity forces. The motion of particles caused the fluid around them to move downwards and the interface to deform. The contact angle on the surface of the particles was held fixed at the specified value of 120º. The particles continued to move downwards even after reaching the equilibrium height z=0.4. When a particle center moved below the equilibrium height, the direction of the capillary force reversed and it acted upwards against the direction of motion of the particle causing it to decelerate. The maximum velocity attained by the particles before deceleration was 7.9 cm/s. The particles reversed their directions for z= 0.36*R*.

The particles also moved apart laterally because of the repulsive hydrodynamic forces. These forces arise since the direction of motion of the particles is perpendicular to the line joining their centers and so the fluid is squeezed through the gap between the particles. The lateral velocity (tangential to the undeformed interface) of the particles reached the maximum value after approximately one complete oscillation of the particles about the equilibrium height, and after that the velocity slowly decreased with time. The maximum lateral velocity was around 0.77 cm/s. The maximum velocity normal to the interface was around 7.9 cm/s, an order of magnitude larger than the lateral velocity. After the vertical oscillations of the particles decayed because of the viscous drag and the repulsive hydrodynamic forces that result from these oscillations became smaller than the attractive capillary forces, the particles reversed directions and started to move towards each other. The attractive forces arise because of the deformation of the interface which in the gap between the particles is greater than on the sides. (The deformation of the interface gives rise to the vertical capillary force that is required to balance the buoyant weight of the particle.) The maximum lateral distance between the particles, before they turned around, was 3.5*R*, i.e., there was an increase of 0.3*R* from the initial distance between the particles. The lateral velocity with which two particles came together increased with decreasing distance.

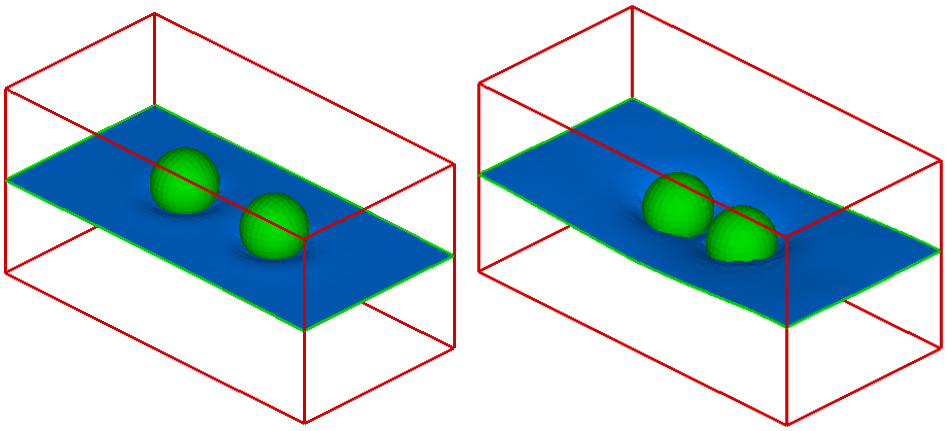

t=0.02 s t=0.26 s

Figure S16. Motion of two particles released at the surface. The radius of particles was 0.1 and the contact angle for the particles was 120º. The initial positions of the particle centers were at a height of 0.95*R* above the undeformed fluid interface. The densities of the particle, and the upper and lower fluids were: 1.1, 0.5 and 1.0 g/cm^3 and the interfacial tension was 4.0 dyn/cm. The interface near the particles deformed to meet the contact angle condition and the vertical capillary force pulled the particles downwards. Initially, the lateral distance between the particles increased. However, as the oscillations normal to the interface decayed and the magnitudes of repulsive hydrodynamic forces decreased, the particles came together under the action of lateral capillary forces.

It is well known that the magnitude of attractive lateral capillary force between two particles depends on their buoyant weights [4,7]. Specifically, the deformation of the interface due to the particles gives rise to the vertical capillary force which is required for balancing the particles buoyant weights. However, since the deformation of the interface in the region between the two particles is greater, there is a lateral component of the capillary forces on the particles which is attractive and causes the particles to come together. We have already noted that our experiments show that the tendency of floating particles to disperse after they were sprinkled onto the interface was greater when the area of intersection of the interface and the particle was greater. Also, the dispersion velocity was larger for the smaller particles. The smaller particles cause a smaller deformation of the interface and so the attractive capillary forces between them are weaker. This is a consequence of the fact that the capillary forces scale as the radius, whereas the buoyant weight scales as the third power of the radius. Therefore, the height or position within the interface of small particles (for which the buoyant weight is negligible) is primarily determined by the contact angle. For example, if the contact angle for a small spherical particle is 90º, it floats so that its center is at the undeformed interface [4,7].

We, therefore, considered the case where the particle density was one half of that of the lower liquid and the contact angle was 85º. Thus, in equilibrium the particles float so that nearly one half of the particle was above the interface. The results for this case are described in Figures SI17 and SI18. As before, the particles were pulled downwards by the vertical capillary forces leading to vertical oscillations. As a result of these oscillations, the two particles moved apart. The amplitude of oscillation decreased with increasing time. In this case, since the particles float without causing significant deformation of the interface, the attractive lateral capillary forces between them were much weaker than in Figure S16. The particles continued to move apart as shown in Figure S18. Simulations were stopped when the distance between the particles was 6.19*R*.

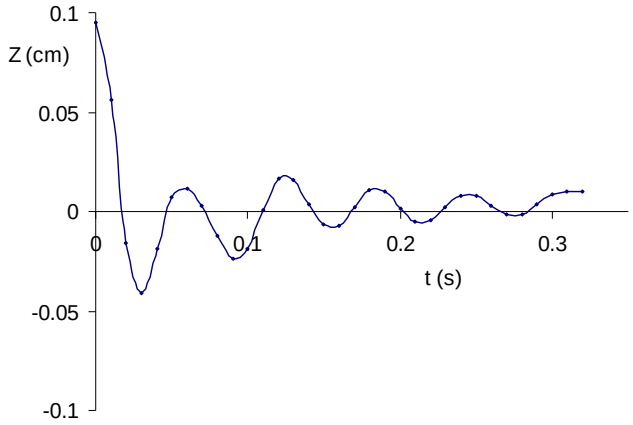

Figure S17. The z-coordinate of the particles, obtained from numerical simulation (DNS), is shown as a function of time. The parameters are the same as in Figure S18. The particle oscillated about the equilibrium height before coming to rest. The amplitude of oscillations decreased with time. The frequency of oscillation was approximately 16.7 Hz.

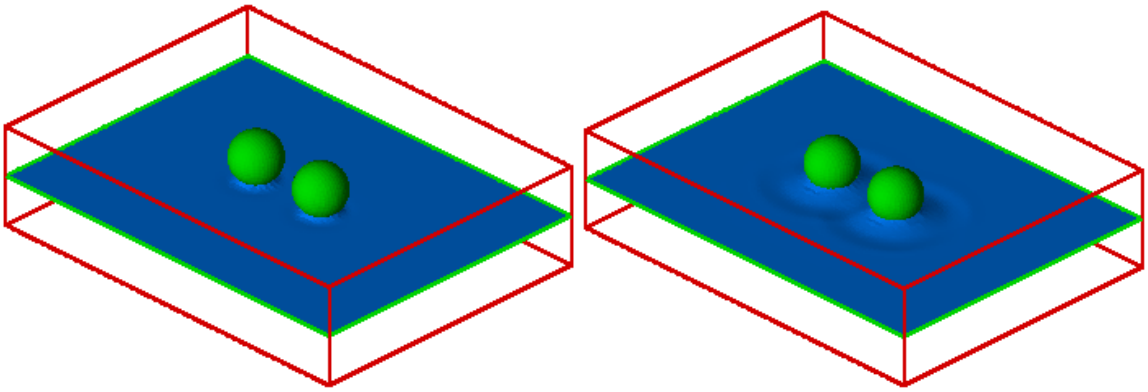

t=0.003 s t=0.005 s

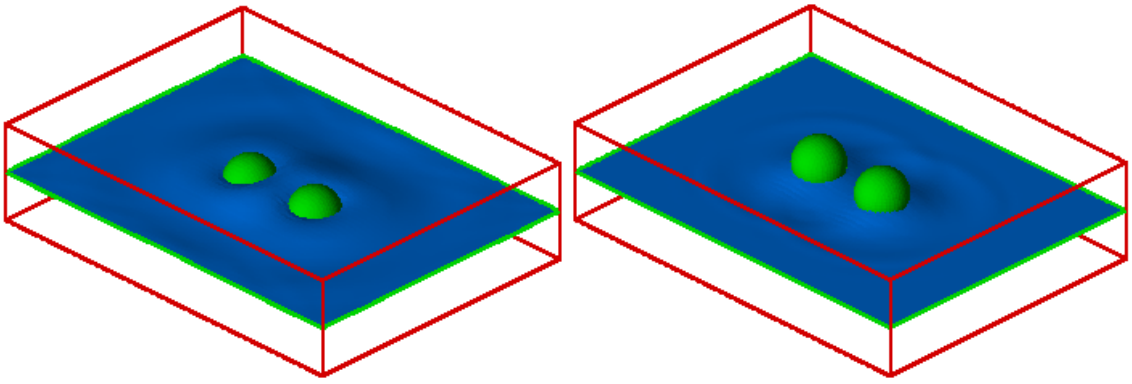

t=0.02 s t=0.06 s

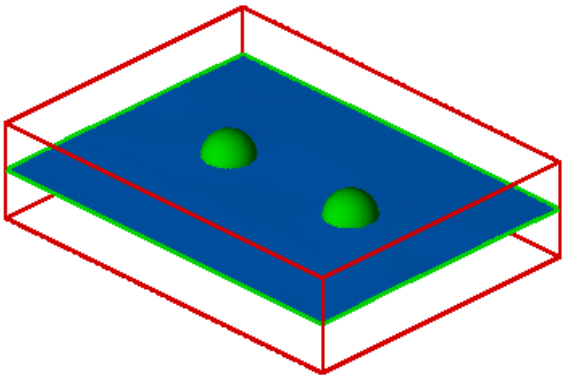

t=0.32 s

Figure S18. Motion of two identical particles. The particle radius was 0.1*R* and the contact angle was 85º. The initial height of the two particles was 0.95*R* above the undeformed fluid interface. The initial lateral distance between the particles was 3.2*R*. The densities of the particle, and the upper and lower fluids were: 0.5, 0.1 and 1.0 g/cm^3 and the interfacial tension was 10.0 dyn/cm. The interface near the particles deformed to meet the contact angle condition. The resulting vertical capillary force pulled the particles downwards. The particles motion also caused the interface to deform and the waves to develop. The resulting fluid velocity caused the two particles to move apart. For the final figure, the distance between the particles was 6.19*R*.

We next describe the case in which one particle was already at its equilibrium height within the interface and the second one was released at a height of 0.95*R* above the equilibrium height. The latter was pulled downwards by the gravity and capillary forces, while the former approximately maintained its vertical height (see Figure S19). The particle that was released above the equilibrium height oscillated about the equilibrium height before coming to rest, but its lateral motion was negligible. However, the particle that was released with its center at equilibrium moved away. This result is similar to that observed in experiments. The lateral

velocity of the particle was about one half of the velocity for the case where both of the particles were released at a height of 0.95*R* above the interface (see Figure S20).

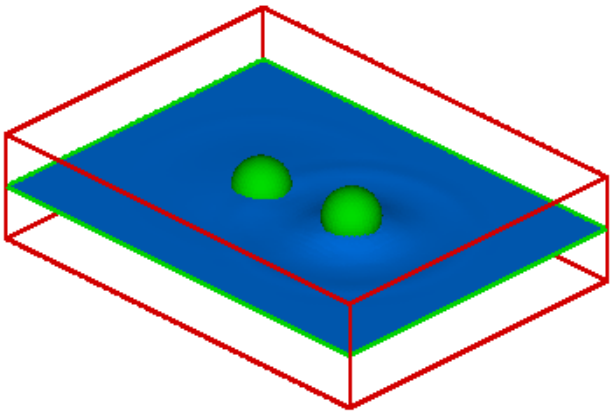

Figure S19. The particle on the left was released at its equilibrium height and on the right was released at 0.95*R* above. The parameters are the same as in Figure S18 and t=0.002 s. The vertical oscillatory motion of the latter particle caused the deformation of the interface. The motion also caused the particle released near the equilibrium position to move away.

We have noted that the lateral velocity with which particles sprinkled onto a liquid surface dispersed increases with increasing number of particles. To study this dependence of the lateral dispersion velocity on the number of particles, we next describe the case of four particles considered in Figure S21. The particles were released at a height of 0.95*R* above their equilibrium position within the interface. The initial positions of the particles formed the vertices of a square with sides 3.2*R*. The initial distance between the neighboring particles was the same as for the two particles case described in Figure S18. The particles were pulled downwards towards their equilibrium height where they oscillated (about the equilibrium height) before coming to rest. The particles also moved apart at the same speed (within numerical errors). Furthermore, the direction of their motion was along diagonals through their centers. The maximum lateral velocity of the particles was about 2.2 times larger than the velocity for two particles (see Figure S20). This is in agreement with the experimental result that the average velocity with which particles moved apart increases with the number of particles dropped. In experiments, the initial locations of the four particles could not be controlled (i.e., the particles centers did not form the vertices of a square), and so the lateral velocities of the particles with which they moved apart were not the same. However, the average velocity for four particles was larger than for two.

The above DNS results show that when a particle is released above its equilibrium height within the interface the vertical capillary force pulls it downwards causing it to accelerate to a

relatively large velocity normal to the interface. Also, since the motion of the particle is inertia dominated, it oscillates several times about its equilibrium height before the viscous drag causes its motion to stop. This motion of nearby particles in the direction normal to the line joining their centers gives rise to the repulsive hydrodynamic forces which cause them to move apart. As the particles velocity in the normal direction to the interface decreases, the magnitudes of the repulsive forces and the dispersion velocity also decrease. Therefore, after some time when the repulsive hydrodynamic forces become smaller than the attractive capillary forces, particles begin to come back together. However, if the buoyant weight of particles is negligible, as is the case for micron and submicron sized particles, then particles only disperse since the attractive capillary forces for them are negligible.

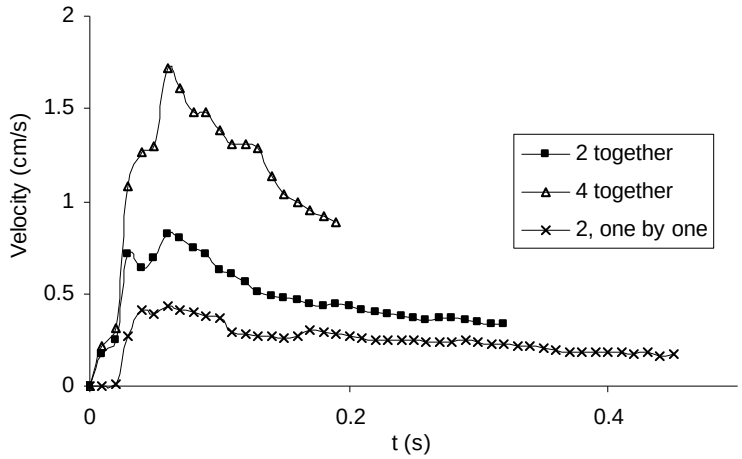

Figure S20. The lateral velocity of the particles is shown as a function of time. The parameters are the same as in Figure S18. The cases shown are: (i) Two particles released together at a height of 0.95*R* above the undeformed interface. The initial distance between the particles was 3.2*R*. (ii) Four particles released together at a height of 0.95*R* above the undeformed interface. The initial positions of the four particles formed the vertices of a square with sides 3.2*R*. (iii) One particle released at a height of 0.95*R* above the undeformed interface, and the center of the second one was at the undeformed interface. The horizontal distance between the particles was 3.2*R*. The velocity of the latter particle is shown. The velocity of the particle released above the undeformed interface was negligible.

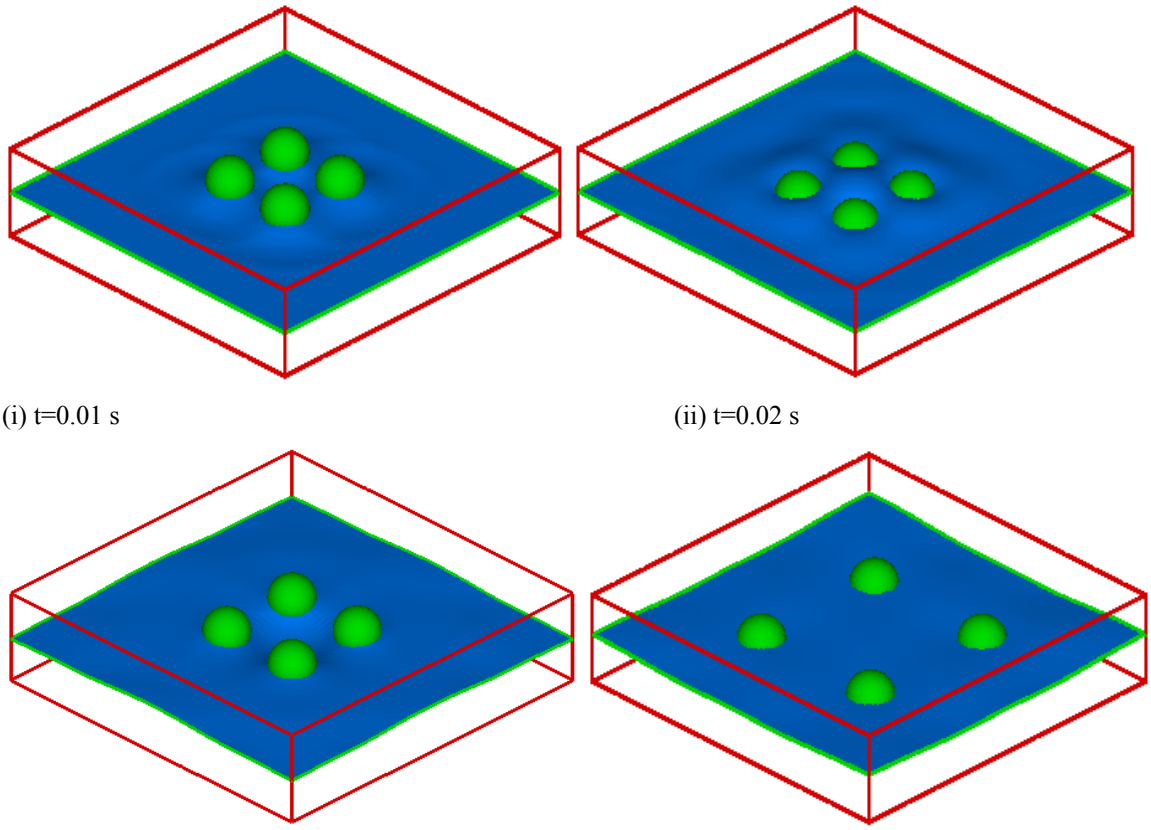

(i) t=0.01 s (ii) t=0.02 s

(iii) t=0.0.05 s (iv) t=0.191 s

Figure S21. (a) Direct numerical simulation of the motion of four particles released above their equilibrium height. The radius of the particles is 1 mm and the initial distance between centers and the undeformed fluid interface was 0.95*R*; the lower 0.*05R* of the particles are immersed. The particles were placed on the four vertices of a square with sides 3.2*R*. The contact angle was maintained at 85º. The other parameters are the same as in Figure S18. The interface near the particles deformed to meet the contact angle condition and the vertical capillary force pulled the particles downwards. The particles oscillated about their equilibrium height generating waves on the interface. The particle centers were above the undeformed interface in (i) and (iii), and below in (ii) and (iv). The lateral hydrodynamic forces that arise because of the particles motion normal to the line joining their centers cause the particles to move away from each other. The distance between neighboring particles in the last figure in the sequence was 6.35*R*.

A.3. Force balance and the equation of motion of a particle

We next consider the forces that act on a particle in the direction normal to the interface when it comes in contact with the interface. These forces cause the particle to move towards its equilibrium position within the interface. The main driving forces for this motion are the vertical capillary force and the particle's buoyant weight. The viscous drag resists the particle's motion. The acceleration of the particle under the action of these forces can be written as:

$$m\frac{\mathrm{d}V}{\mathrm{d}t} = \mathrm{F_{st}} + \mathrm{F_D} + \mathrm{F_g}\,, \tag{1}$$

where m is the effective mass of the particle which includes the added mass contribution, V is the particle velocity, $\mathrm{F_{st}}$ is the vertical capillary force, $\mathrm{F_D}$ is the drag, and $\mathrm{F_g}$ is the gravity force.

We next write the acceleration term in the above equation in terms of the particle's vertical displacement s, i.e.,

$$\frac{\mathrm{d}V}{\mathrm{d}t} = \frac{\mathrm{d}V}{\mathrm{d}s}\frac{\mathrm{d}s}{\mathrm{d}t} = V\frac{\mathrm{d}V}{\mathrm{d}s} = \frac{\mathrm{d}\left(\frac{V^2}{2}\right)}{\mathrm{d}s}\,.$$

Here s is measured such that s=0 corresponds to the position in which the particle just touches the interface. Using this in (1), we have

$$m\frac{\mathrm{d}\left(\frac{V^2}{2}\right)}{\mathrm{d}s} = \mathrm{F_{st}} + \mathrm{F_D} + \mathrm{F_g}\,. \tag{2}$$

We next integrate the above equation with respect to s, from the particle's initial position (s=0) to the present position s

$$m\left(\frac{V^2}{2} - \frac{V_0^2}{2}\right) = \int_0^s \mathrm{F_{st}}\,ds + \int_0^s \mathrm{F_D}\,ds + \int_0^s \mathrm{F_g}\,ds\,, \tag{3}$$

where V_0 is the initial velocity of the particle. The left side of this equation gives the change in the kinetic energy of the particle, and the terms on the right side respectively represent the work done by the vertical capillary, drag and gravity forces.

The work done by the vertical capillary force can be written in terms of the change in the interfacial energy of the system

$$\int_0^s \mathrm{F_{st}}\,ds = \Delta A_{12}\,\gamma_{12} - A'_{1p}\,\gamma_{1p} + A_{1p}\,\gamma_{1p} + A_{2p}\,\gamma_{2p}\,. \tag{4}$$

Equation (4) assumes that the particle is initially immersed in the upper fluid denoted by subscript "1" and the total surface area of the particle is denoted by $A_{1p}^{'}$, γ_{ip} is the surface tension between the i[th] fluid and the particle, A_{ip} is the particle's surface area wetted by the i[th] fluid, ΔA_{12} is the decrease in the surface area between the upper and lower fluids because of the presence of the particle on the interface, and γ_{12} is the interfacial tension between the upper and lower fluids. The energy due to the line tension is assumed to be negligible. It is easy to show that when the deformation of the interface because of the presence of the particle is negligible [17] for a spherical particle of radius *R* the above expression reduces to

$$\int_0^s \mathrm{F_{st}}\, ds = \pi R^2 \gamma_{12}\left(1+\cos\theta\right)^2 \tag{5}$$

where θ is the contact angle, as defined by Young's equation: $\cos\theta = \dfrac{\gamma_{p2}-\gamma_{p1}}{\gamma_{12}}$. The drag force acting on the particle, and thus also the work done by the drag, depends on the particle's velocity. Assuming that the drag is given by the Stokes' law, the work done can be written as:

$$\int_0^s \mathrm{F_D}\, ds = -\int_0^s 6\pi R\mu V\zeta\, ds = -6\pi R\mu \int_0^s V\zeta(s)\, ds\,. \tag{6}$$

Here μ is the viscosity of the lower fluid and $\zeta(s)$ is a factor that accounts for the dependence of the drag on the fraction *s* of the particle that is immersed in the lower and upper fluids, and the viscosities of the fluids involved. The functional form of $\zeta(s)$ is not known. Also, notice that the velocity *V* varies as the particle moves normal to the interface. In this work, the Stokes law is used to estimate drag, but other appropriate drag laws can also be used.

The work done by the gravity force is approximately given by

$$\int_0^s \mathrm{F_g} ds = \mathrm{Q}\left(\rho_\mathrm{p} - \rho_\mathrm{c}\right)\mathrm{g}\, s \tag{7}$$

where Q is the particle volume, ρ_c is the effective fluid density which changes with *s* while the particle moves normal to the interface, and ρ_p is the particle density.

After substituting (5), (6) and (7) in (3), we obtain

$$m\left(\frac{V^2}{2}-\frac{V_0^2}{2}\right)= \pi R^2\gamma_{12}\left(1+\cos\theta\right)^2 - 6\pi R\mu\int_0^s V\zeta(s)\,ds + \mathrm{Q}\left(\rho_\mathrm{p}-\rho_\mathrm{c}\right)\mathrm{g}\,s\,. \tag{8}$$

The above equation for the particle velocity can be simplified further by assuming that the initial kinetic energy of the particle is negligible and using the trapezoidal rule to evaluate the integral term. The former is valid for our experiments because the height from which particles were dropped was only a few millimeters and the particle size was small. If we assume that the drag arises primarily from the portion of the particle immersed in the lower liquid, which for simplicity we will assume to be one half, and $\zeta(s)$=1/2. Then, after simplification, we obtain

$$m\frac{V^2}{2}= \pi R^2\gamma_{12}\left(1+\cos\theta\right)^2 - \frac{6}{4}\pi R\mu Vs + \mathrm{Q}\left(\rho_\mathrm{p}-\rho_\mathrm{c}\right)\mathrm{g}\,s\,. \tag{9}$$

We next assume that the particle floats so that its center is at the undeformed interface and the effective mass $m = \frac{4}{3}\pi R^3\rho_p$. For this case, $\theta=\frac{\pi}{2}$ and $s = R$. The latter assumes that the particle reaches this position for the *first* time. If the particle oscillates about the vertical position, the distance travelled by the particle will be larger and so will be the work done by the drag force. Using these approximations in the above equation, after simplification, we obtain

$$R\rho_p V^2 = \frac{3}{2}\gamma_{12} - \frac{9}{4}\mu V + 2R^2\left(\rho_\mathrm{p}-\rho_\mathrm{c}\right)\mathrm{g} \tag{10}$$

If the interface between the two fluids does not remain flat, then there is an increase in the interfacial area between the two fluids which must be accounted for in expression (4). Moreover, if a spherical particle floats (in equilibrium) such that its center is not at the interface, then ΔA_{12} is smaller than πR^2. The interfacial energy available for conversion to the kinetic energy (a fraction of which is acquired by the particle) is smaller for this case. This is consistent with our experimental observation that the dispersion velocity was larger for the particles that floated such that the contact line was near their equator.

The solution *V* of the above quadratic equation is given by:

$$V=\frac{-\frac{9}{4}\mu+\sqrt{\frac{81}{16}\mu^2+4R\rho_p\left(\frac{3}{2}\gamma_{12}+2R^2\left(\rho_\mathrm{p}-\rho_\mathrm{c}\right)g\right)}}{2R\rho_p} \tag{11}$$

Equation (11) gives the particle's velocity after its center reaches the undeformed interface for the *first* time.

Notice that equation (11) implies that the influence of gravity on the velocity decreases with decreasing particle radius. For sufficiently small particles, the velocity increases with decreasing radius and with increasing surface tension, and decreases with increasing viscosity. For example, for $\mu = 0.001$ Pa.s, $\rho_p = 1000.0$ kg/m^3, $\rho_p - \rho_c = 0.1$ kg/m^3 and $\gamma_{12} = 0.07$ N/m, the dependence of the particle velocity on the radius is shown in Figure S22. For R=100 μm, V=1.01 m/s, and for R=100 nm, V=23.05 m/s. The figure shows that when R is smaller than 1 mm the velocity increases with decreasing particle radius. The latter is an expected result because the capillary force acting on a particle varies linearly with the radius whereas the particle's mass varies as the third power of the radius. Therefore, the velocity attained by a particle due to the capillary force increases with decreasing particle radius. In the limit R approaching zero, the velocity is given by

$$V = \frac{2\gamma_{12}}{3\mu}. \tag{12}$$

This is the maximum velocity that can be attained by a particle under the action of the vertical capillary force. For the air-water interface, the maximum velocity attainable (under the assumptions stated above) is 46.67 m/s.

The above velocity can be used to estimate the time taken to move a particle initially touching the interface to a position where its center is at the undeformed interface; for R=100 μm, the time taken is of O(10^{-4}) s, and for R=1 μm, it is of O(10^{-7}) s.

It is noteworthy that the work done by the drag force is significant only when the particle moves over a much longer distance, the fluid viscosity is relatively large, or the velocity is sufficiently large; otherwise the decrease in the interfacial energy due to the capture of the particle at the interface is mostly converted into the kinetic energy. The velocity for this can be obtained from (10) by neglecting the drag and gravity terms, which gives

$$V = \sqrt{\frac{3\gamma_{12}}{2R\rho_p}}. \tag{13}$$

Equation implies that the particle velocity increases with decreasing particle radius, and in fact diverges as the radius approaches zero. However, since the work done by the drag force increases with increasing particle velocity, the velocity for small particles does not diverge, but is given by the balance of the viscous drag and the vertical capillary force. Furthermore, if the fluid viscosity

is sufficiently large, the particle velocity remains small and the particle does not oscillate before coming to a state of rest. Thus, particles sprinkled onto the surface of a very viscous liquid are less likely to disperse.

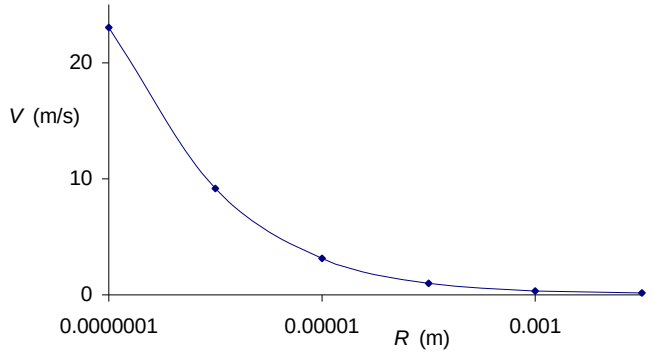

Figure S22. The velocity of a spherical particle normal to the interface given by equation (11) is plotted as a function of the particle radius. The parameter values were assumed to be: $\mu = 0.001$ Pa.s, $\rho_p = 1000.0$ kg/m^3, $\rho_p - \rho_c = 0.1$ kg/m^3 and $\gamma_{12} = 0.07$ N/m.

We remind the reader that the above analysis assumes that the equilibrium position of the particle center is at the undeformed interface and that the interface around the particle is flat. If, however, the interface around the particle is not flat, the decrease in the area between the upper and lower fluids due to the presence of the particle will be smaller than the area of intersection between the particle and the flat interface and the discrepancy must be included in equation (11). An increase in the interfacial area between the fluids due to the deformation of the interface implies that the interfacial energy available to drive the motion of the particle is smaller, and thus the maximum velocity attained by the particle will be smaller. Furthermore, even if interface around the particles is flat at equilibrium, this may not be the case when it reaches this position for the first time because the particle and the fluid velocities are not zero and as a result the interface contains waves. The interface can become flat only after both the particle and the fluid stop moving.

Our direct numerical simulations show that the particle oscillates about the equilibrium several times before coming to rest (see Figure S17). This is due to the fact that the motion of particle is inertia dominated. Thus, when the particle reaches the equilibrium height, its velocity is non-zero, and so it continues to move downwards. However, when the particle center moves below the equilibrium height, the vertical capillary force changes direction and acts upwards to bring the particle back to the equilibrium. The viscous drag acts throughout this process to slow the particle.

To study the above behavior of the particle motion, we consider equation (1) for the motion of the particle. We will use the approximations stated above to simplify (1), i.e., those used for obtaining (10). The surface tension force will be obtained by assuming that the particle is spherical and that the contact angle is equal to its equilibrium values. The drag force will be assumed to be given by the Stokes formula, as discussed above, and the buoyancy force only depends on the particle's vertical position. Under these assumptions, equation (1) can be written as

$$m\frac{\mathrm{d}V}{\mathrm{d}t} = -2\pi\left(R\sin\theta_c\right)\gamma_{12}\sin\left(\theta_c+\alpha\right) - 6\pi\mathrm{R}\mu V\zeta(s) + \mathrm{Q}\left(\rho_\mathrm{p} - \rho_\mathrm{c}\right)\mathrm{g} \qquad (14)$$

Here θ_c is the angle between the vertical and the contact line on the sphere's surface and α is the contact angle.

A time dependent numerical solution of the above differential equation is shown in Figure S23. The parameter values used were the same as for the numerical results presented in Figure S17. The figure shows that the particle oscillates about the equilibrium height several times while the amplitude of the oscillations decays with time because of the viscous drag. These results are qualitatively similar to those in Figure S17a obtained using the DNS approach. However, there are also some differences. The frequency of oscillation given by the two approaches differed by about 7% and the rate of decay of oscillations was slower for the DNS results. This perhaps is due to the fact that the interface is allowed to deform in the DNS approach, but is assumed to be flat in the derivation leading to (14). The interface, as shown in Figure 3, deforms because of the vertical oscillations of the particles.

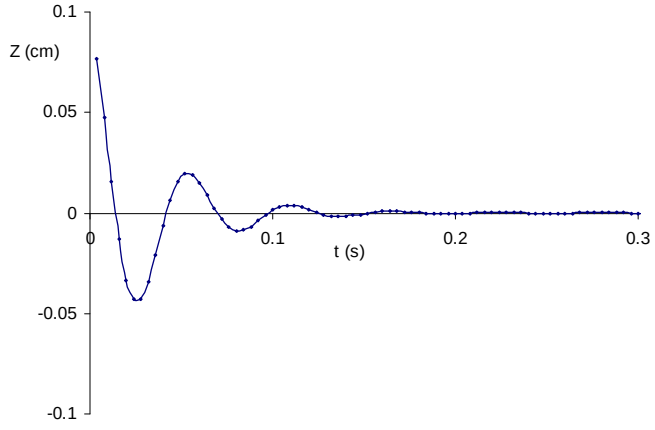

Figure S23. The z-coordinate of the particle center obtained numerically by solving (14) is shown as a function of time. The radius of particle is 0.1 cm. Initially, the particle center is at z=0.95*R* (above the interface). The remaining parameters are the same as in Figure S18. The particle oscillates about the equilibrium position (z=0) before coming to rest. The amplitude of oscillations decreases with increasing time. The frequency of oscillation is approximately 17.9 Hz.

Equation (14) is a linear ODE with variable coefficients. To show that it is equivalent to the equation for a spring-dashpot system, we linearize (14) about the equilibrium position, z=0. To do this, we will assume that the contact angle $\alpha=\frac{\pi}{2}$, $\theta_c=\frac{\pi}{2}$ and $\zeta(s)=1/2$. After linearization, we obtain

$$\frac{4}{3}R^3\rho_p\frac{\mathrm{d}^2Z}{\mathrm{d}t^2} + 3\mathrm{R}\mu\frac{\mathrm{dZ}}{\mathrm{d}t} + 2\gamma_{12}Z + R^2\left(\rho_\mathrm{p} - \rho_\mathrm{c}\right)\mathrm{g}\,\mathrm{Z} = 0. \tag{15}$$

where *Z* is the particle's position. The above second order linear ODE is equivalent to a spring-dashpot system. Its solution can be written as:

$$Z = Z_0 e^{kt} \tag{16}$$

where

$$k = \frac{-3R\mu \pm \sqrt{D}}{\frac{8}{3}R^3\rho_p}$$

$$D = 9R^2\mu^2 - \frac{16}{3}R^3\rho_p\left(2\gamma_{12} + R^2\left(\rho_\mathrm{p} - \rho_\mathrm{c}\right)g\right)$$

The nature of the solution depends on the sign of discriminant *D*. If the sign is positive, then *k* is real and negative for both of the roots. In this case, the solution decays exponentially with time to zero. This is expected to be the case when the fluid viscosity is sufficiently large. If the sign of *D* is negative, then *k* is complex. The solution is oscillatory with the frequency of oscillation $\omega = \sqrt{-D}/2\pi$. The real parts of both of the roots are negative and so both of the solutions decay exponentially to zero. The time constant τ of the solution, i.e., the time taken by the solution to decay by a factor of e^{-1}, is given by

$$\tau = \frac{8R^2\rho_p}{9\mu} \qquad (17)$$

The time constant decreases with decreasing particle size and with increasing viscosity. Therefore, the vertical oscillations of a trapped particle decay faster when the radius is smaller and the viscosity is larger. Using the parameter values in Figure S22, we find that for a particle of radius 1 mm, the time constant is 0.9 s, and for a 10 μm sized particle it is $9.0\text{x}10^{-5}$ s. We remind the reader that the former estimate of the time constant is smaller than for our direct numerical simulations for which the interface is allowed to deform. Also notice that as R becomes small there is a critical value of R for which D becomes positive. For these parameter values, the critical value of R is 12 nm. The imaginary part of the root gives the frequency of oscillation. For the parameter values listed in figure S22, the frequency of oscillation (ω) in Hz is plotted as a function of the particle radius in figure S24. The frequency increases with decreasing particle radius. For R=1 mm, ω = 51.6 Hz, and for R=10 μm, ω =$5.2\text{x}10^4$ Hz. The frequency for R=1 mm is in a qualitative agreement with the value for our experimental data.

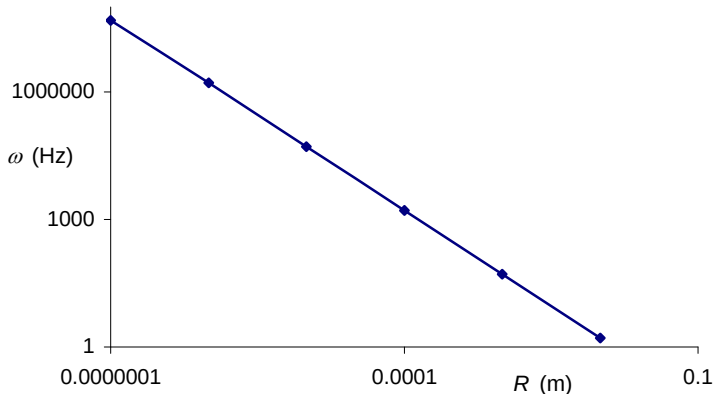

Figure S24. The frequency (ω) of oscillation of the solution given by equation (16) is plotted as a function of the particle radius. The parameter values are the same as in figure 22.

A.4. Conclusions

It is shown that when a particle comes in contact with a liquid surface it is pulled into the interface towards its equilibrium height by the vertical capillary force and that during this process the particle can accelerate to a relatively large velocity normal to the interface. For example, a particle of radius 100 μm sprinkled onto the water surface may attain a velocity of the order of 1

m/s. The maximum velocity on an air-water interface, which increases with decreasing particle size, can be as large as ~47 m/s. It is also shown that a particle being adsorbed oscillates about its equilibrium height before coming to rest under viscous drag. These oscillations of the particle cause the fluid around it to move away which in our experiments was measured using smaller tracer particles that were present on the liquid surface.

When two or more particles are dropped simultaneously onto the surface their motion in the direction normal to the interface (and to the line joining their centers) gives rise to the strong repulsive hydrodynamic forces which cause them to move apart. The velocity with which particles move apart increases with increasing number of particles. Also, smaller sized particles disperse more readily because the importance of interfacial forces increases with decreasing particle radius. An analysis of the particle's equation for the vertical motion is used to determine the dependence of the velocity on the factors such as the fluid viscosity, the change in the interfacial energy due to the adsorption of the particle, the particle radius and the buoyant weight. The viscous drag causes the oscillatory motion of particles about their equilibrium heights to decay with time, and thus the repulsive hydrodynamic forces that arise because of this motion also decrease with time. As a result, after reaching a maximum value, the velocity with which particles move apart decreases with time. Furthermore, if the buoyant weight of particles is not negligible, e.g., 200 μm sized sand particles used in Figure 1, they also experience attractive lateral capillary forces that arise because of the deformation of the interface. Although these attractive lateral forces are relatively weaker, after the repulsive hydrodynamic forces become smaller they cause particles to come back to cluster. The velocity with which particles come back to cluster however is much smaller. Micron and nano sized particles, on the other hand, remain dispersed since for them the attractive capillary forces are negligible.